Aalto University

OPEN ACCESS

This is an electronic reprint of the original article.
This reprint may differ from the original in pagination and typographic detail.

Shi, Xuetong; Meng, Yang; Bi, Ran; Wan, Zhangmin; Zhu, Ya; Rojas, Orlando J.

Enabling unidirectional thermal conduction of wood-supported phase change material for photo-to-thermal energy conversion and heat regulation

Published in:
Composites Part B: Engineering

DOI:
10.1016/j.compositesb.2022.110231

Published: 01/10/2022

Document Version
Publisher's PDF, also known as Version of record

Published under the following license:
CC BY

Please cite the original version:
Shi, X., Meng, Y., Bi, R., Wan, Z., Zhu, Y., & Rojas, O. J. (2022). Enabling unidirectional thermal conduction of wood-supported phase change material for photo-to-thermal energy conversion and heat regulation. *Composites Part B: Engineering*, *245*, Article 110231. https://doi.org/10.1016/j.compositesb.2022.110231

This material is protected by copyright and other intellectual property rights, and duplication or sale of all or part of any of the repository collections is not permitted, except that material may be duplicated by you for your research use or educational purposes in electronic or print form. You must obtain permission for any other use. Electronic or print copies may not be offered, whether for sale or otherwise to anyone who is not an authorised user.

Composites Part B 245 (2022) 110231

Contents lists available at ScienceDirect

Composites Part B

journal homepage: www.elsevier.com/locate/compositesb

Enabling unidirectional thermal conduction of wood-supported phase change material for photo-to-thermal energy conversion and heat regulation

Xuetong Shi [a,b], Yang Meng [b,c,**], Ran Bi [a], Zhangmin Wan [a], Ya Zhu [b], Orlando J. Rojas [a,b,*]

[a] Bioproducts Institute, Department of Chemical & Biological Engineering, Department of Chemistry and Department of Wood Science, The University of British Columbia, 2360 East Mall, Vancouver, BC V6T 1Z3, Canada
[b] Department of Bioproducts and Biosystems, School of Chemical Engineering, Aalto University, Espoo, 02150, Finland
[c] Yunnan Provincial Key Laboratory of Energy Saving in Phosphorus Chemical Engineering and New Phosphorus Materials, The Higher Educational Key Laboratory for Phosphorus Chemical Engineering of Yunnan Province, Kunming University of Science and Technology, Kunming, 650500, PR China

ARTICLE INFO

Keywords:
Wood
Phase change material
Boron nitride
Solar energy conversion
Thermal energy storage
Layer-by-layer assembly

ABSTRACT

Phase change materials (PCMs) enable passive thermal management by minimizing energy waste. However, a limitation of organic PCMs is their low thermal conductivity, which leads to uneven phase transitions. Herein, we introduce a composite following a green and simple synthesis strategy that uses wood's fiber anisotropy and microporosity to support an organic PCM (polyethylene glycol, PEG). We first incorporate exfoliated boron nitride (BN) and polyethylenimine (PEI) in a layer-by-layer (LbL) assembly followed by capping with conductive polypyrrole. This modification of the wood framework endows non-leaking filling with PCM and simultaneous light absorption and thermal conduction. The loaded BN provides enhanced thermal conductivity, 4.4 and 26 times higher compared to neat PEG and delignified wood. As a result, the multicomponent system is effective for solar-to-thermal energy conversion with a latent heat of melting of up to ~160J/g (~78% PEG encapsulation). Moreover, the modified wood composite shows thermal durability and stability for at least 50 heating and cooling cycles. Overall, we take advantage of unidirectional heat transport for light conversion and storage and demonstrate the operation principle using a proof-of-concept prototype system.

1. Introduction

Phase Change Materials (PCMs) allow thermal energy storage (TES) and can be used to convert solar radiation, absorb excess environmental heat, as well as store and release thermal energy. Combined with the possibility for temperature regulation, PCM systems have attracted interest for sustainable thermal energy utilization [1–5]. This is possible given the high thermal (latent) energy involved during phase transition. For their use in TES systems, PCMs should ideally display a high latent heat storage density and good chemical stability. For these purposes, noncorrosive organic PCMs have been considered, including paraffins, fatty acids, fatty acid esters as well as organic polymers [6–8]. All of these PCMs show great value for thermal management but display a low thermal conductivity (k) and are prone to leakage upon melting. These factors limit the efficiency of heat transfer, energy storage and release [9,10]. To address these issues, conductive fillers have been proposed, including carbon nanotubes [11], nanomagnetite [12], expanded graphite [13,14], graphene oxide [15], carbon black [16], and aluminum oxide nanoparticles [17]. Unfortunately, poor compatibility and phase separation of mixtures of such fillers with PCMs lead to low performance and uneven heat distribution, especially after cycling operation [17–19]. Therefore, new strategies are required in designing PCM-based systems for long-term stability and uniform heat transfer.

Shape-stabilization of PCMs by encapsulation in a supporting matrix [20] is a possible route to reduce leakage. For this purpose, supporting matrices for TES have included metal-organic frameworks (MOFs) [21], carbon aerogels [22,23], mesoporous silica [24,25], and polymers [26,27]. Meanwhile, environmental factors such as sustainability and

* Corresponding author. Bioproducts Institute, Department of Chemical & Biological Engineering, Department of Chemistry and Departments of Wood Science, 2360 East Mall, The University of British Columbia, Vancouver, BC V6T 1Z3, Canada.
** Corresponding author. Yunnan Provincial Key Laboratory of Energy Saving in Phosphorus Chemical Engineering and New Phosphorus Materials, The Higher Educational Key Laboratory for Phosphorus Chemical Engineering of Yunnan Province, Kunming University of Science and Technology, Kunming, 650500, PR China.
E-mail addresses: mengyang@kust.edu.cn (Y. Meng), orlando.rojas@ubc.ca (O.J. Rojas).

https://doi.org/10.1016/j.compositesb.2022.110231
Received 21 June 2022; Received in revised form 5 August 2022; Accepted 14 August 2022
Available online 19 August 2022
1359-8368/© 2022 The Authors. Published by Elsevier Ltd. This is an open access article under the CC BY license (http://creativecommons.org/licenses/by/4.0/).

biodegradability are of great significance. Hence, wood has been tested as a promising three-dimensional support for thermal management; for this purpose, an additional feature is wood's vertically aligned and interconnected hierarchical tubular fibers [28,29]. The capillary effects and surface interactions between the cellulosic porous scaffold and organic PCM contribute to leakage-proof encapsulation [30,31]. As such, this wood-stabilized PCM has been proposed for thermal energy storage [32–37]. Unfortunately, the low thermal conductivity of wood limits effective heat storage and release [38]. Though wood haven been utilized in PCM systems to approach better sustainability [35–37], a higher thermal conduction still needs to be realized to ensure an efficient utilization of latent heat. Hence, the incorporation method, mechanism as well as the loading of thermal enhancer filler in the PCM composite system are subjects that need special consideration. Additionally, a process that is typically used in related efforts, *i.e.,* lignin removal, significantly reduces light absorption in the visible and ultraviolet light spectrum. The poor photo-absorption ability of wood (or delignified wood) as well as that of the PCM reduce the conversion efficiency of solar irradiation and limit applications in the field of solar-to-thermal energy management [39].

In this study, we address the above limitations by introducing a simple strategy that uses a wood-based PCM composite that exhibits high thermal conductivity and efficient light-to-thermal energy conversion. For this purpose, controlled wood delignification is used to increase the free volume for PCM infiltration while allowing high hemicellulose retention, to preserve the mechanical stability of wood [40]. Meanwhile, hexagonal particles of boron nitride (BN) are incorporated as a low-cost filler to endow high thermal conductivity [41]. This enables heat transfer pathways in an adiabatic process involving the 3D interconnected structure of wood facilitating heat energy storage and release. Simultaneously, an efficient photothermal energy conversion is added by *in-situ* polymerization of cationic pyrrole (producing polypyrrole, PPy), which enhances light absorption and electrical conductivity. BN and PPy were effectively grown inside wood by electrostatic assembly. Compared with methods such as wood carbonization [42–45] or loading with Fe_3O_4 particles [12,46] and MOFs [47], for instance, to capture and convert solar energy, our modification is realized by following simple steps and processing in aqueous media, at room temperature. In sum, light adsorption capacity and light-to-thermal energy conversion are demonstrated in a multifunctional wood-supported PCM composite.

2. Experimental

2.1. Materials

Boards of balsa were purchased from Modulor, Berlin, Germany. Sodium chlorite ($NaClO_2$, ≥90%), polyethylenimine (PEI, Mn = 10000 by GPC, branched), pyrrole (≥98%), poly(ethylene glycol) (PEG, Mn = 6000 g/mol), iron(III) chloride hexahydrate ($FeCl_3 \cdot 6H_2O$), boron nitride (powder, size around 1 μm, 98%), isopropanol(IPA, ≥98%) were purchased from Sigma-Aldrich.

2.2. Liquid exfoliation of boron nitride, BN

BN powder (5 g) was mixed with 500 ml isopropanol for 14 h at 800 rpm (magnetic stirrer). Then the dispersion was sonicated in a water bath at 80 °C for 10 h. These steps were repeated 8 times to exfoliate the BN and to obtain a well-dispersed BN suspension.

2.3. Delignified wood and LbL deposition

The balsa samples (with two different sizes, 2x2x0.5 cm and 10x3x0.5 cm) were delignified by treatment with 1 wt% $NaClO_2$ aqueous solution at 100 °C with the pH of the solution adjusted to 4.6. The resulting, delignified wood (DW) showed an off-white color.

DW was modified by adsorption of boron nitride (herein termed as BN-modified wood, BW) following layer-by-layer (LbL) deposition. For this purpose, the samples of delignified wood (DW) were immersed overnight in cationic PEI (3 mg/ml) solution. The samples were then washed and immersed in a 10 mg/ml BN dispersion for 10 min. The negatively charged BN adsorbed on the cationic PEI forming a strongly adsorbed layer. The samples were then washed with de-ionized (DI) water. Some samples were immersed again in 3 mg/ml PEI solution for 10 min and rinsed with DI water. To form multilayers of PEI/BN, the process was repeated 2, 5, 10 and 15 times. Part of samples were freeze-dried for further use. The BW subjected to the above treatments are thereafter referred to as BW2, BW5, BW10 and BW15, where the numeral refers to the respective number of PEI/BN layers.

Additional experiments were carried out with BW capped with PPy (termed PW). More specifically, the BW samples (BW2, BW5, BW10 and BW15) were immersed in a 1 M pyrrole aqueous solution for 24 h. A total amount of 1 M $FeCl_3.6H_2O$ was then added to initiate *in-situ* polymerization to produce PPy. After reaction for 24 h, PW samples were washed with DI water and freeze-dried for further use. These samples were named as PW2, PW5, PW10 and PW15.

2.4. Impregnation with the PCM (PEG)

The prepared BW and PW wood samples were immersed in PEG using a vacuum oven (−0.1 MPa, 80 °C), following our earlier procedure [32]. The BW samples filled with PEG are designated as BW2@PEG, BW5@PEG, BW10@PEG and BW15@PEG and those with PPy capping layer are referred to as PW2@PEG, PW5@PEG, PW10@PEG and PW15@PEG.

2.5. Structural, morphological, chemical, and thermal characterization

The zeta potential of PEI, BN and pyrrole were determined by using a Malvern Zetasizer (Nano ZS90) analyzer. The morphologies of the wood samples were observed by scanning electron microscopy (SEM) using a Zeiss Sigma VP scanning electron microscope (Germany) and a Hitachi S2600 N Variable Pressure SEM (Japan). The UV absorption was measured with a Shimadzu (UV-2600 with ISR-2600Plus) Integrating Sphere. The thermal properties of the samples were studied by differential scanning calorimetry (TA instruments MT-DSC Q2000) operated at 5 °C/min heating/cooling rate, from 25 °C to 80 °C under a nitrogen atmosphere (50 ml/min flow rate). Two replicates of each group were tested following three heating-cooling cycles. The average values of six experiments were determined. Thermal conductivity was measured with a C-Therm TCi™ Thermal Conductivity Analyzer. The specific heat capacity was determined by using a TA instrument (DSC Q1000) with sapphire calibration and the thermal conductivity was reported at a temperature of 23 °C. Fifty consecutive thermal cycles were conducted from 20 °C to 80 °C (TA instrument DSC Q1000) at a heating/cooling rate of 5 °C/min under a nitrogen atmosphere (50 ml/min flow rate). The thermal stability and degradation of the samples were studied by using thermogravimetric analysis on a TA instrument (TGA Q5500). The samples were heated from 30 °C to 650 °C at 10 °C/min rate, under a 60 ml/min nitrogen gas flow. FTIR measurements were conducted for composition analysis using a PerkinElmer spectrometer (Spectrum Two FT-IR spectrometer) using the wavenumbers between 500 and 4000 cm^{-1} with a resolution of 32 cm^{-1}. X-ray diffraction (XRD) patterns of the samples were measured in the 2θ range of 3°–80° with CoKα radiation on a Bruker D8 Advance Bragg-Brentano diffractometer. The photothermal energy conversion was determined by exposing the samples to an infrared lamp (120 V AC, 600 W, US) and real-time monitoring of using of the temperature evolution using an IR (FLIR, T620) camera.

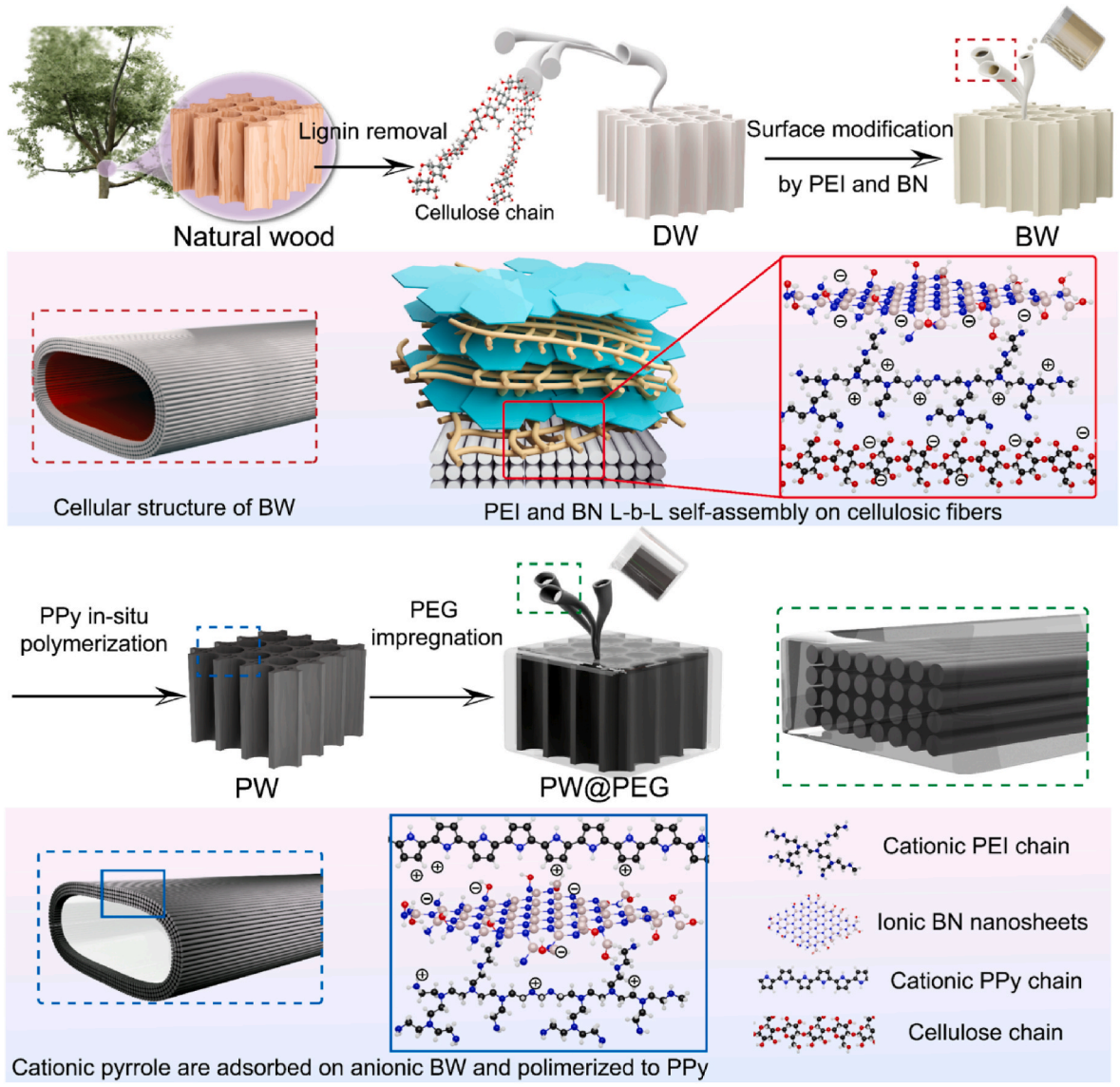

Fig. 1. Schematic illustration of the procedure used for the synthesis of BW, PW and PW@PEG. PEI/BN LbL assembly on DW was carried out using 2, 5, 10 and 15 LbL cycles, yielding the respective BW. PPy was synthesized on BW to form the thermally conductive PW samples, which were further infiltrated with the phase change material, PEG.

3. Results and discussion

3.1. Wood modification and loading

The procedure used for surface modification on balsa as well as the designated PCM composites is illustrated in Fig. 1. Balsa (*Ochroma pyramidale*) is highly porous (the tracheid content is as high as 90%) and lightweight (±87.7 mg/cm^3). Delignification created large void volumes, not only from the cell wall but from the middle lamella and cell corners (Fig. S2), which allowed extensive PCM infilling [32]. After the removal of lignin, the residual hemicelluloses contributed to the anionic character of the delignified wood sample (-COO$^-$ surface groups) [48]. When immersed in water, the inner structures of wood displayed features typical of anionic hydrogels.

We note that BN nanosheets obtained by sonication-assisted hydrothermal exfoliation (Fig. S3) presented a negative zeta potential (−14.6 mV), which enabled adsorption following the LbL strategy with PEI (+15.2 mV) interlayers. In addition, the outmost anionic BN facilitated adsorption of the capping cationic pyrrole (+12.1 mV in aqueous dispersion) by electrostatic interactions. On the other hand, the hydroxyl groups on the defective edges of the BN [49–52], promoted hydrogen bonding with PEI and cellulose in the BW samples. After fully infiltration of pyrrole, the addition of Fe^{3+} initiated the *in-situ* polymerization [53]. In these PW samples, hydrogen bonding also occurred between PPy's amine groups and the hydroxyl groups of BN (Fig. 1).

3.2. Morphology of conductive BW, PW and PW@PEGs

The wood structures were preserved after the LbL self-assembly (PEI/BN) and after deposition of PPy (BW, PW and PW@PEG, Fig. 2a–g). The off-light yellow color of the BW samples (Fig. 2e), developed upon PEI/BN immersion, was taken as qualitative indication of the effect of PEI adsorption. The efficient BN adsorption was confirmed by the observation of the mineral nanosheets attached on the wood tracheid surfaces, as evidenced in SEM images taken in the longitudinal and radial directions of PW15 after 15 adsorption cycles (Fig. 2b, e and 2e1), which were contrasted with the neat, clean and smooth cell wall surfaces typical of DW (Fig. 2a and d). An increased number of BN nanosheets accumulated and stacked on the cell wall surface with the number of cycles (Figure S4b1-b3 and S4c1-c3) which is

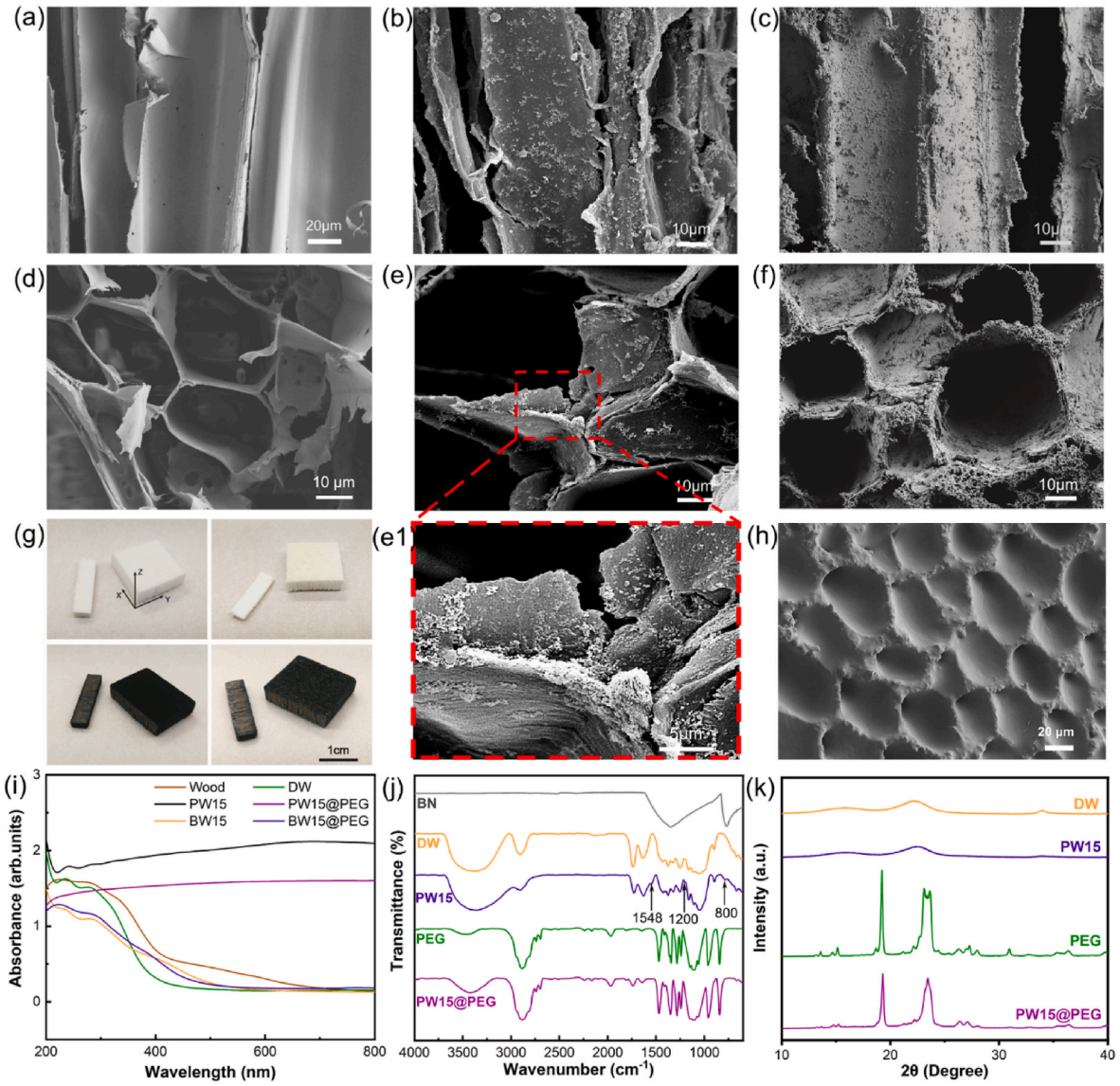

Fig. 2. SEM of the longitudinal section of (a) DW. (b) BW15, and (c) PW15. SEM of the radial morphology of (d) DW, (e) BW15 and (e1) BW15 at an increased magnification as well as (f) PW15. (g) Photos of DW (top left), BW15 (top right), PW15 (bottom left) and PW15@PEG (bottom right), (h) SEM of the radial morphology of PW15@PEG. (i) UV and (j) FTIR spectra of the respective samples, as indicated and (k) XRD of DW, BW10, PW15 and PW15@PEG.

attributed to the role of the PEI interlayer, which indicates a thermally conductive material.

The effectiveness of BN loading was confirmed by TGA measurements conducted with the BW samples, Fig. S5. Additionally, FTIR results indicated the effective adsorption of BN in DW (Fig. S4a). To endow efficient light-to-thermal energy conversion, PPy was applied on the BW samples, given PPy light absorption capacity [29]. The capping PPy covered the PEI/BN layers and changed the surface roughness in both the radial and longitudinal directions (Fig. 2c and f). Compared with the surface of BW and neat DW (Fig. 2a, b, d and e), the addition of PPy increased the surface roughness, which enhances the interfacial interactions with the infiltrated PEG [54]. The surface features or protuberances observed in Fig. 2c and f, provides a better molecular contact in PW15, which increases the work of adhesion and encapsulation of PEG.

The rough surface of the PW samples (Figure S4d1-d3 and S4e1-e3) facilitates multiple light scattering, absorption and energy harvesting [28]. Additionally, the dark color imparted by PPy in PW and PW@PEG samples, enhances light absorption (Fig. 2i). Besides its photothermal conversion effect, the PPy capping layer protects the thermally-conductive boron nitride particles in the PW samples. The system guarantees light-capture by wood following simple and low-energy processing.

3.3. PCM-loaded systems

For thermal energy storage, PEG was applied as a source of latent heat in PW@PEG. After the impregnation of PEG in PW *via* vacuum infiltration, the lumina were filled completely, as seen in the fully covered lumen shown in Fig. 2h. For PW15, the appearance of peaks at 1548 cm^{-1} and 1200 cm^{-1} corresponded to the pyrrole ring C═C and C–N stretching vibrations [28,29], confirming the presence of PPy. The peaks around 800 cm^{-1} (B–N stretching vibration) and 1380 cm^{-1} (B–N bending vibration) [55,56] are indicative of the presence of BN in PW. On the spectrum of PW15, the characteristic peaks at 3337 cm^{-1}, 1736 $cm^{-1}$and 1032 cm^{-1} are assigned to the stretching vibration of O–H, C═O and C–O valence vibrations of cellulose, respectively [32,57], indicating that the chemical composition of wood was preserved after both physical adsorption and *in-situ* polymerization of PPy on the surface. However, the absorbance values corresponding to C═O and C–O

Table 1
Phase change properties and energy storage efficiency (F).

Sample	*Tm* (°C)	*ΔHm* (J/g)	*Tc* (°C)	*ΔHc* (J/g)	*F* (%)
PEG6000	62.4	204.5	40.21	187.7	100
PW2@PEG	62.2 ± 0.5	159.7 ± 7.3	41.7 ± 0.3	153.0 ± 4.5	78.1%
PW5@PEG	62.2 ± 0.9	154.3 ± 10.9	40.6 ± 1.0	149.5 ± 6.9	75.4%
PW10@PEG	61.7 ± 0.3	156.4 ± 12.5	42.7 ± 0.5	149.6 ± 11.6	76.5%
PW15@PEG	61.9 ± 1.0	139.2 ± 13.2	42.4 ± 1.0	133.9 ± 11.4	68.1%

Note: *F* (%) is the effective melting enthalpy content, which can be calculated as.

were reduced and that of O–H was broadened in PW15, which imply the formation of hydrogen bonds after surface modification. The adsorption of BN and PPy rely on secondary interactions including electrostatic attraction between oppositely charged surfaces and hydrogen bonding. The spectrum of PW15@PEG (Fig. 2j) showed the characteristic peaks of PEG and PW. No new peaks were observed in PW15@PEG, indicating that no chemical reactions took place. Meanwhile the reduced absorbance from 3300 cm^{-1} to 3600 cm^{-1} corresponded to the O–H stretching vibration typical of the formation of hydrogen bonds by the addition of PEG (Fig. 2j). The chemical compatibility and structural stability of PW and PW@PEG were also confirmed by XRD analyses. The typical crystalline peaks of cellulose I at 2θ = 14.9°, 16.5°, 22.5° and 34°, were assigned to the (101), (10–1), (020) and (040) crystal planes, respectively [58,59], which remained in the PW samples, Fig. 2k. No new crystal peaks appeared in the PW samples, confirming the physicochemical stability of the systems with the given BN loading, Fig. 2k and Fig. S7. After the incorporation of PEG, Fig. 2k, the characteristic peaks of PW15@PEG corresponded to the superposition of PW15 and PEG, confirming the preservation of the crystal structures of the initial materials and the chemical compatibility of the system.

3.4. Thermal energy storage of PW@PEG

The phase change and thermal energy storage properties of the

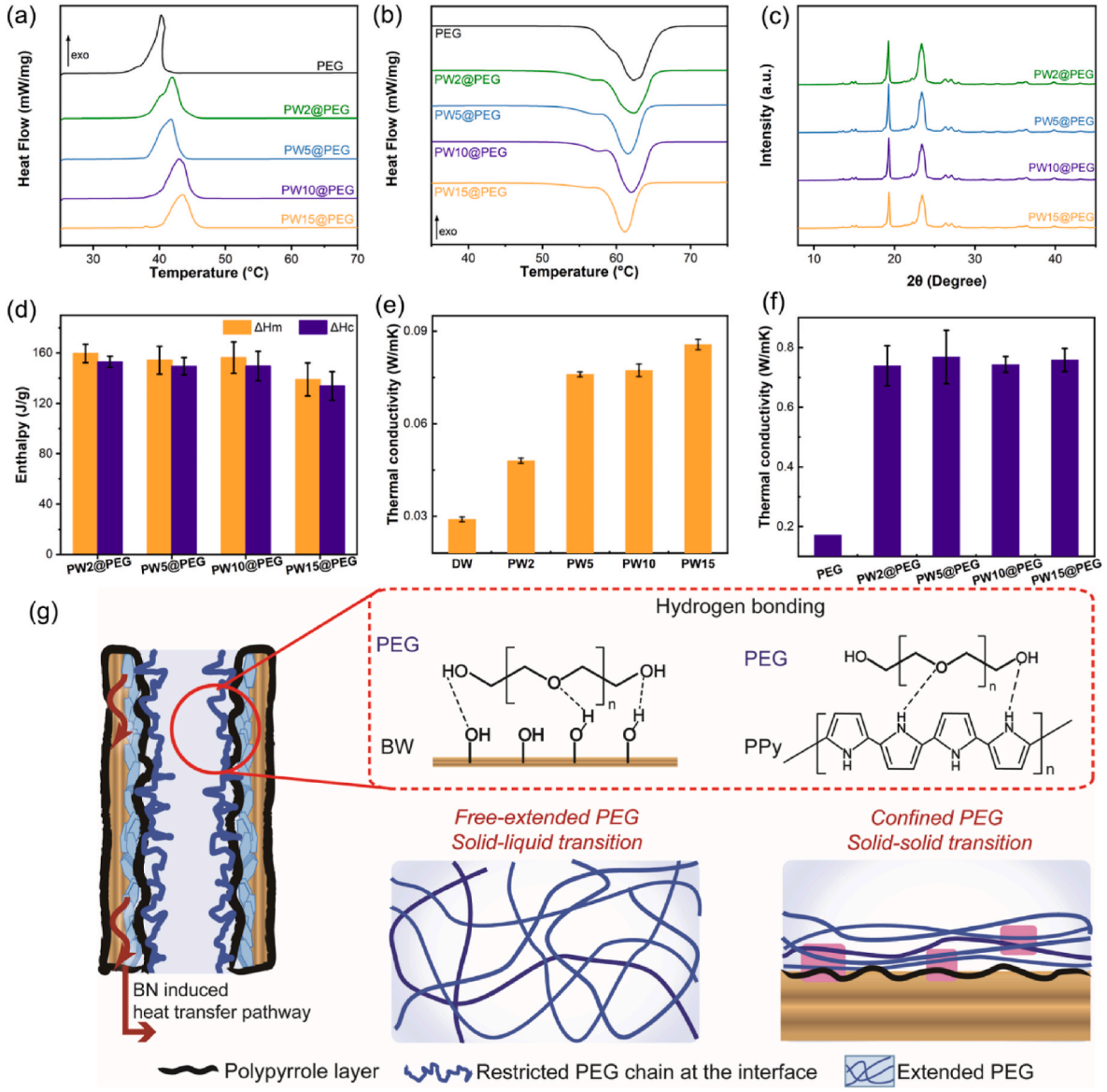

Fig 3. DSC thermograms for PW@PEG upon (a) heating and (b) cooling. (c) The latent heat of heating and cooling in PW@PEGs. (d)Schematic illustration of the interactions and hydrogen bonding between the components. (e) Longitudinal thermal conductivity of the PWs modified with BN and DW. (f) Longitudinal thermal conductivity of PW@PEGs and pristine PEG. (g) Molecule interactions in PW@PEG and the PEG chain motion during phase transition.

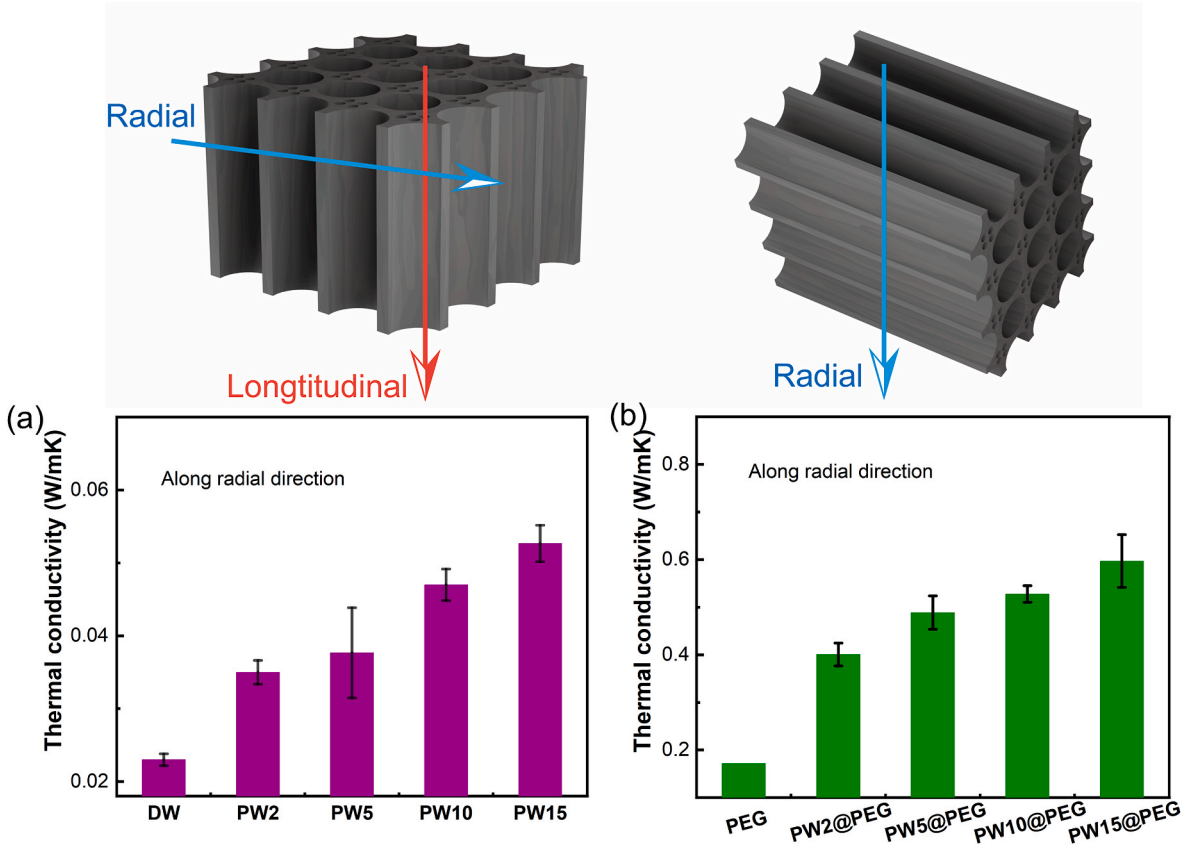

Fig. 4. Thermal conductivity along the radial direction of (a) PWs modified with BN and DW, as well as those of (b) PW@PEGs and pristine PEG.

samples are next discussed in terms of the phase transition temperature and latent heat, Table 1. The latent heats of melting (*ΔHm*) and crystallization (*ΔHc*) of neat PEG are 204.5 J/g and 187.7 J/g, respectively. Incorporated in a supporting matrix, wood, the PEG in PW@PEG showed no leakage (Fig. 2g) and had a similar phase change performance compared to that of neat PEG. The results indicate a successful solution to the PCM leakage problem without compromising the thermal energy storage performance.

PEG infilling mainly relied on capillary forces acting in the lumina and the hydrogen bonding [32] between PEG and the surface of PW. The amino groups of PPy and the hydroxyl groups of DW together with the edges of exfoliated BN participated in hydrogen bonding (Fig. 3g) and facilitated the interaction with PEG, achieving a high encapsulation efficiency (FTIR, Fig. 2j and S6).

$$F(\%) = \frac{\Delta Hm \text{ of PWX@PEG}}{\Delta Hm \text{ of PEG}} * 100\%$$

The PEG loaded in the PW samples showed a high phase change enthalpy (*ΔHm* = 159.7 J/g) with 78.1% efficiency (*F*) in PW2@PEG. With the addition of BN, the enthalpy of melting and cooling as well as the encapsulation efficiency were reduced (Fig. 3d), which is explained by the reduced space and pore volume available for PEG diffusion and the increased number of BN/PEI layers. Additionally, PEG chains were confined in the wood scaffold by surface interaction so that not all PEG undergoes solid to liquid transition, producing a loss of fractional enthalpy [60], as illustrated in Fig. 3g. Furthermore, the higher molecular contact area given by the rough, outermost surface of the wood framework constrains PEG chains near the cell wall, so that a higher adhesion energy and hydrogen bonding result in a less extended PEG molecules during phase change [21]. Therefore, the reduced impregnation volume of PEG with the increased BN loading as well as the lower fraction of extended PEG chains produced a lower latent heat of melting (from 159.7J/g to 139.2J/g) and cooling (from 153.0 J/g to 133.9J/g).

Compared to the values of neat PEG, PW@PEG samples showed a reduced *Tm* and an increased *Tc*. The interconnected three-dimensional wood matrix provided sites for PEG to crystallize, serving as nucleating sites during cooling. The phase change temperature was slightly affected by BN loading (Fig. 3a and b, Table 1): a reduced *Tm* and improved *Tc* were observed for samples PW2@PEG-PW15@PEG, as seen in the shift of peaks shown in the DSC profile. This favorable effect of BN on phase transition relied on the enhanced thermal conductivity, which accelerated both the melting and crystallization processes. Additionally, upon melting (Fig. 3b), the PEG in contact with BN engaged in effective heat absorption (given the enhanced heat transfer of BN) compared to the wider range of melting temperature of in pure PEG. With BN loading endowed a more effective heat absorption (shortened melting process) (Fig. 3b). The PW@PEG structures are well maintained, presenting stable crystal structures and chemical properties depending on BN adsorption cycles (Fig. 3c).

3.5. Thermal conductivity

The thermal conductivity of the PW and PW@PEG samples was measured and compared with the references (DW and PEG), Table S1, Fig. 3e and f. Generally, cellulosic materials are insulating [61] and DW exhibited a low thermal conductivity (23 °C), ~0.029 W/(m·K) in the longitudinal direction. This value increased (0.086 W/(m K) by the effect of BN, a figure that is ~3-fold higher compared to that of DW (Fig. 3e). After the incorporation of PEG, the axial thermal conductivity was measured to be 0.758 W/(m·K), which is 4.41 times greater than the value of neat PEG (0.177 W/(m·K)) and 26-fold higher than that of DW. The improved thermal conductivity is explained by the effect of BN, and the increased *k* in PW@PEG, which scaled with BN loading. Additionally, the growth of BN along the anisotropic wood lumina ensures an

Table 2
Comparison of thermal conductivity reported for related similar phase change composites.

Wood-supported PCMs	Thermal Conductivity (W/mK)	*Refs*
Delignified wood/capric acid-palmitic acid	0.49	[30]
Wood powder/paraffin-PEG/graphite	0.32	[35]
Wood/PEG/SiO_2	0.33	[36]
Wood powder/n-octadecane/SiO_2/BN	0.73	[37]
Carbonized wood/PEG/Fe_3O_4	0.23	[42]
Carbonized wood/1-tetradecanol	0.67	[45]
PPy-modified wood/PEG/BN	0.76	This study

effective unidirectional heat transfer in the longitudinal direction (note the lower *k* in radial direction for all samples with a maximum of 0.597 W/(m·K), Fig. 4 and Table S3). This indicates an improved thermal conduction *via* the LbL strategy. As reported previously (Refs. [51,55,62]), BN has been broadly and effectively employed as a filler for heat management. In this study, BN was applied in a layer-by-layer format along the natural wood lumina providing unidirectional heat transfer pathways (as illustrated in Figs. 3g and 4). Moreover, the enhanced *k* was attributed to the reduced thermal interface resistance [39], due to the improved adsorption and interfacial interactions of PPy. Compared to the PWs and with the same amount of BN loading, the higher thermal conductivity in all PW@PEGs is explained by the removal of air and the closing of pores in PCM composites, given PEG infiltration. Compared with previously reported wood-stabilized PCM systems (Table 2), the thermal conductivity in the present study is the highest.

3.6. Thermal durability and stability

The thermal resistance of DW was improved by the treatments (PW@PEG degradation occurred at higher temperature, Fig. 5a and S9a). As depicted in Fig. 5a, the PW@PEG samples with different BN loading exhibited similar decomposition: first partial degradation at around 250–350 °C and a second stage with degradation at ~400 °C. The BN material is thermally resistant [62] as there is negligible pyrolysis losses at 650 °C (Fig. 5a). A higher percentage of residual mass at 650 °C was measured with BN loading, 4.74 and 7.98% for PW2@PEG and PW15@PEG, respectively. This increased char is attributed to the incorporated BN and the lower volume of PEG in the material.

The thermal degradation temperature of the PW@PEG samples was around 400 °C, which indicated a good thermal stability, and a slightly delayed decomposition of PW@PEG with increased BN loading (Fig. S9a). Besides the thermal resistance of BN, interactions between PEG and the cellulose surface modified with PPy, BN and PEI contributed to the improved thermal stability. The effect of PPy as a protective barrier against the degradation of cellulose was also a factor.

PW10@PEG showed the best performance considering the thermal conductivity (Fig. 3f) as well as the latent heat stored in the samples (Fig. 3d and Table 1). The durability of PCM composites is an important consideration, i.e., to ensure stable performance and avoid phase separation or loss of properties. To examine the long-term applicability,

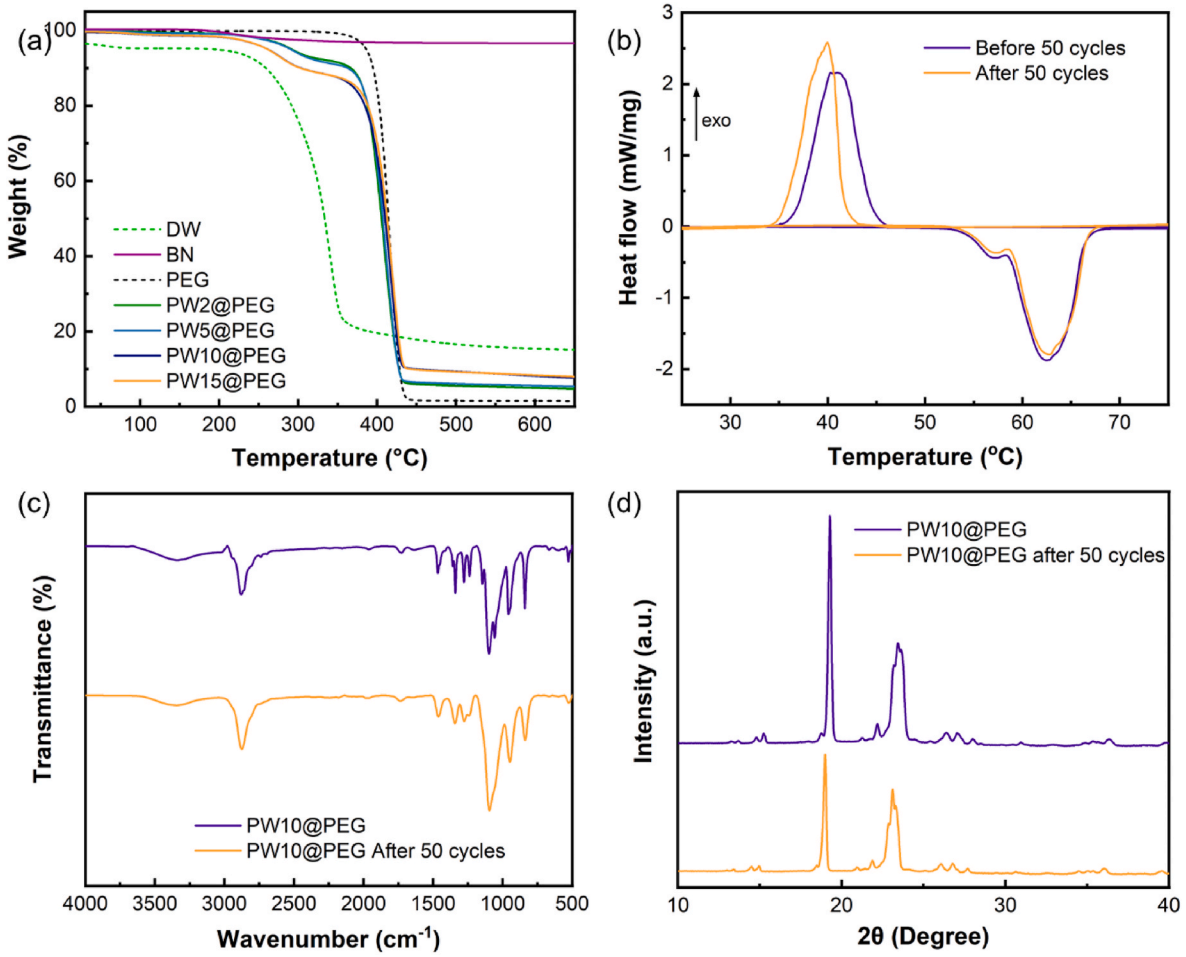

Fig. 5. (a) Thermogravimetric analysis (TGA) of DW, PEG and PW@PEG for given BN modification cycles. Stability and recyclability of PW10@PEG before and after 50 consecutive cycles of heating and cooling as observed by (b) DSC; (c) FTIR and (d) XRD measurements.

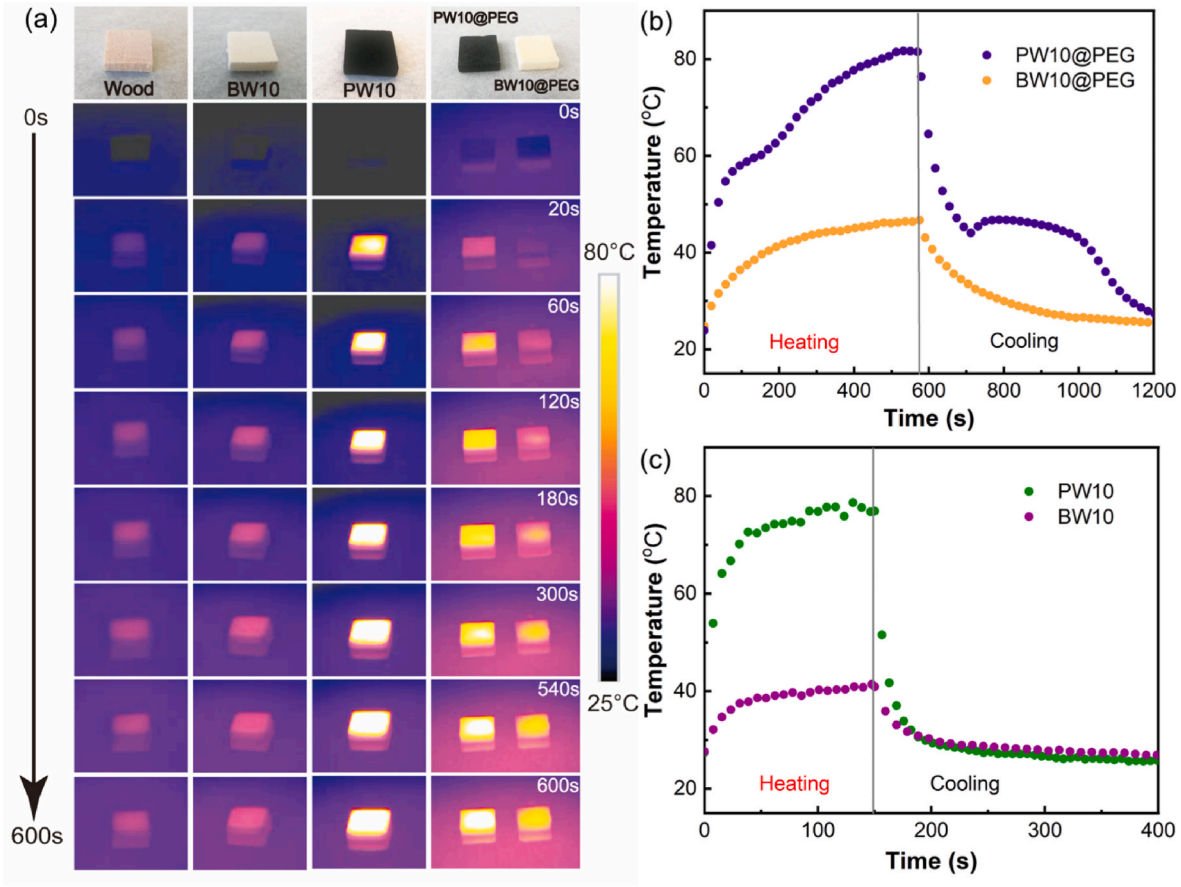

Fig. 6. (a) Images acquired with an IR camera of natural wood, BW10, PW10, BW10@PEG and PW10@PEG after illumination for 600s. (b–c) Temporal changes at the surfaces of BW10, PW10, PW10@PEG and BW10@PEG.

PW10@PEG was consecutively heated and cooled for 50 cycles and the phase change performance as well as the compositional properties were examined. As shown in Fig. 5b and Fig. S9b, there was no significant evolution of latent heat (Table S2) and the similar phase change performance indicated good thermal durability and repeatability. The partial enthalpy loss may be caused by the strong interactions between PEG and PW, which enabled segmental free-extended PEG chains [60]. The compositional stability was studied by FTIR and XRD (Fig. 5c and d), which indicated no significant variation in the profiles after 50 thermal cycles. The preservation of the crystal structure and negligible chemical degradation of the material indicated a great stability and prospects for cyclic use as thermal energy storage system. The repeatable and cycling thermal and physiochemical performance support our observation of good compatibility of the system and the success fabrication of PW@PEG with the incorporation of BN.

3.7. Light-to-thermal energy conversion

We examined the light absorption ability as well as the thermal performance of natural wood, PW10 and PW10@PEG (BW10 and BW10@PEG). Images obtained with an infrared camera were recorded with samples exposed to an infrared lamp (temperature−time profiles, Fig. 6a–c). Consistently, a higher light absorption capacity and more efficient performance were observed for PW10 and PW10@PEG. With the addition of PPy, the surface temperature reached 70 °C within 50 s (Fig. 6a–c). By contrast, natural wood and BW showed a limited temperature gain after much longer times, 600 s (Fig. 6a). As shown in Fig. 7c, PW and PW@PEG led to a significantly high temperature rise. This was not the case in the absence of the PPy capping layer. The efficient light-to-thermal conversion performance is mainly attributed to the high efficiency of photon capture provided by PPy [63]. Additionally, compared to natural wood the improved thermal conductivity of BW10 accelerated the rate of temperature raise (Fig. 6a). As illustrated in Figs. 3g and 7g, BN and PPy were uniformly distributed in the channels of the continuous three-dimensional wood network. This modification endowed heat conversion from light and a heat transfer pathway to enable uniform phase transition and effective thermal energy storage from solar irradiation.

The capping PPy layer was effective for light absorption and allowed light-to-thermal energy conversion. As shown in Fig. 6b and c, both PW and PW10@PEG experienced a rapid temperature raise, within a few seconds, from 20 °C to 55 °C. It is noteworthy noting that PW10@PEG experienced a plateau at around 60 °C and the temperature was maintained for a period of time before the onset of change. This performance indicated the ability to regulate the temperature and to keep the temperature constant by avoiding abrupt heat evolution when PW@PEG underwent phase transition [60]. The thermal energy storage plateau was also shown in the cooling process at 40–45 °C interval, when the light was turned off (Fig. 6b). This phenomenon was not obvious for BW10@PEG because the poor photothermal energy conversion. To examine the application of PW@PEG for temperature regulation, we used a wooden construction model (Fig. 7a and Fig. S10) and followed the real-time indoor temperature in the system containing a roof of natural wood, PW, DW@PEG and PW10@PEG and under infrared light. As shown in the simulation set-up (Fig. S10), the roof of the commercial plywood house model was replaced by the developed PCM composites and exposed to infrared light (600 W, to simulate sunlight) and the interior temperature were recorded when the light was on and off. The working mechanism of the functionalized wood-based roof is illustrated in Fig. 7b. The efficient photothermal conversion and rate of

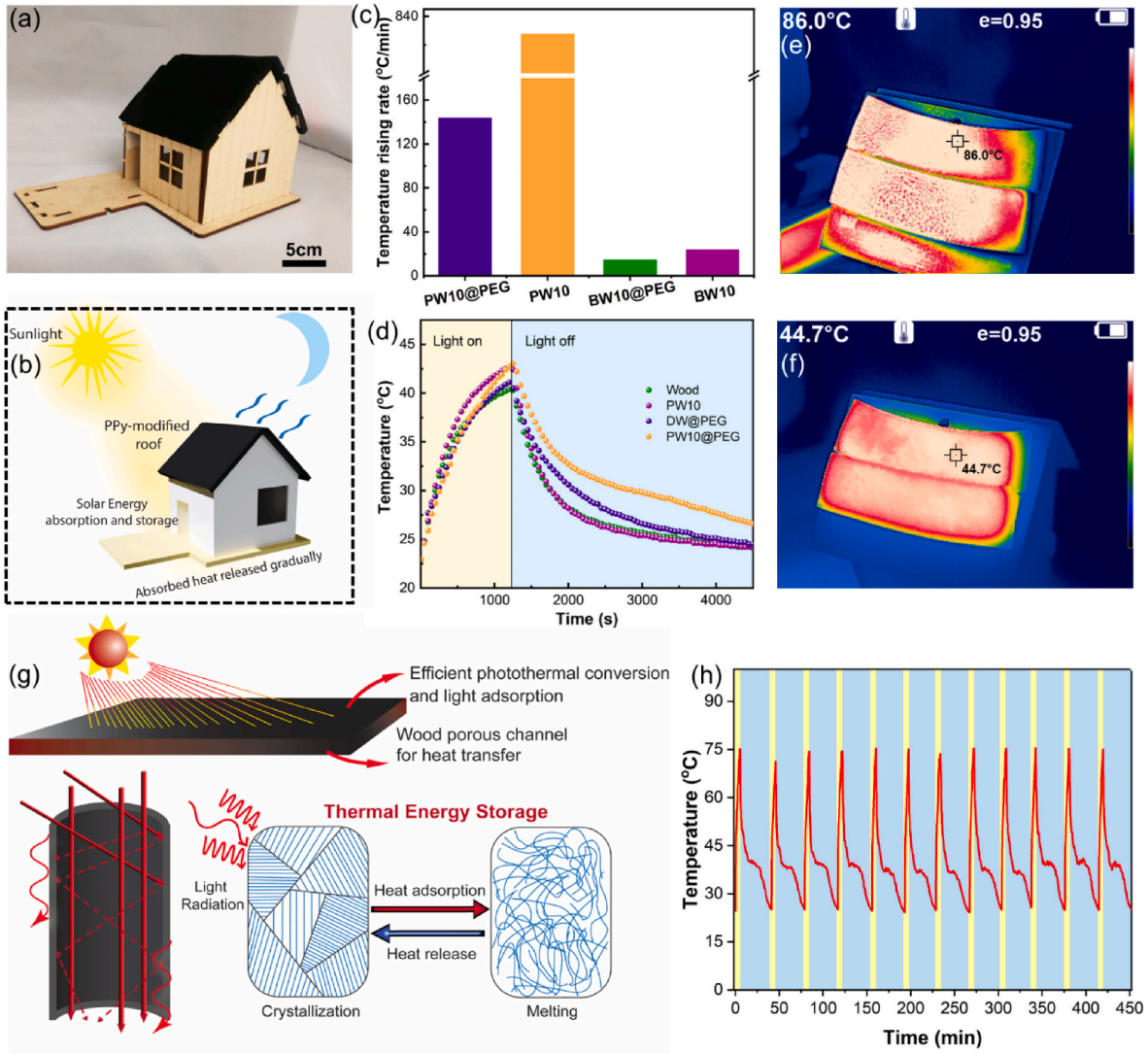

Fig. 7. (a)A wood model house equipped with a roof made from PW@PEG. (b) Illustration of the effect of PW@PEG enabling an enhanced photothermal conversion, solar energy storage and thermal regulation. Efficient photothermal conversion ability and thermal energy storage performance characterized by (c) a temperature increasing rate (wood with and without PPy), (e) temperature of PW@PEG roof model after illumination for 8 min and (f) after 15 min, when light is turned off. (d) Real time indoor temperature change in the model house covered with different roof materials when the model (with and without illumination under a simulated sunlight). (g) Mechanism of PPy-modified wood-supported PCM enabling efficient thermal energy absorption and release. (h) 12 cycles of heat absorption and release in PW@PEG while light is turned on and off.

temperature increase (Fig. 7c) of PW@PEG wooden roof leads to a temperature rise to 80 °C within 8 min illumination, as recorded by IR camera (Fig. 7e). The absorbed heat in PW@PEG is released slowly and, therefore, maintains a warm environment for long periods of time (Fig. 7f, T is maintained at ca. 40 °C after 15min without heating). The interior temperature is also examined to study the potential for temperature regulation. PW10@PEG underwent fast temperature raise and showed the longest heat preservation (Fig. 7d), which is attributed to the PPy layer and the thermal energy storage capacity of the infilled PCM. In contrast, the inner room temperature rapidly decreased to 23 °C with the wood and PW roof (Fig. 7d): the absence of PEG prevented thermal energy absorption as latent heat. By contrast, the latent heat of PW10@PEG was released gradually, maintaining a warm indoor environment, given the improved thermal insulation. The fast light absorption property of PW and PW10@PEG confirmed that PPy acted as effective light-to-thermal energy component. In PW10@PEG, the interconnected 3D wood network modified with BN and PPy served as a thermal diffusion pathway that enabled uniform PEG melting/crystallization, as illustrated in Fig. 7g. Using this material with thermal energy storage performance, the room temperature can be regulated by reducing the heat loss (Fig. 7b, d). After 12 cycles of heating/cooling, PW@PEG exhibited reliable and repeatable thermal energy storage and heat regulation performance (Fig. 7h). So, the proposed wood modification strategy guarantees an improved heat absorption and release performance during the phase change process. Solar to thermal energy conversion and storage in construction materials can be facilitated by the proposed wood modification, leading to energy saving and temperature regulation.

4. Conclusions

A functional wood-based PCM composite is introduced following a simple and low-energy process based on layer-by-layer assembly. BN was employed to enhance the thermal conductivity and was effectively attached to the wood scaffold *via* hydrogen bonding and electrostatic interactions. A capping PPy layer enabled efficient light-to-thermal energy conversion. The distinct three-dimensional wood structure modified with self-assembled BN and PPy was effective in encapsulating PEG

and preventing its leakage; simultaneously, the system endowed a heat transfer path that guaranteed uniform temperature distribution. The latent heat of melting of PW10@PEG reached up to 159.7 J/g for a 78.1% PEG encapsulation efficiency. The thermal conductivity of PW was improved, about 3-times higher compared to DW. The PW10@PEG material showed enhanced thermal conductivity, up by 4.4 times compared with neat PEG and 26 times compared to DW. The thermal stability, durability and chemical reliability after 50 consecutive cycles of heating and cooling suggest PW@PEG as a potential candidate for light-to-thermal energy conversion and storage.

Author contributions statements

Xuetong Shi: Conceptualization, methodology, experiments, data analysis, writing original draft. Ran Bi, Zhangmin Wan and Ya Zhu: Discussion, experimental, illustration and editing. Yang Meng: Conceptualization, discussion, review and editing. Orlando J. Rojas: Supervision, conceptualization, review and editing, funding acquisition.

Declaration of competing interest

The authors declare that they have no known competing financial interests or personal relationships that could have appeared to influence the work reported in this paper.

Data availability

The data that has been used is confidential.

Acknowledgements

The authors acknowledge funding from the Canada Excellence Research Chair Program (CERC-2018-00006), and Canada Foundation for Innovation (Project number 38623) as well as the European Research Council (ERC) under the European Union's Horizon 2020 research and innovation program (grant agreement No 788489). Y.M. acknowledges funding from the China Postdoctoral Science Foundation (NO. 2022MD713757). We are thankful for access to the Nanomicroscopy Center in Aalto University and the UBC Bioimaging facility (RRID: SCR_021304). We also thank Prof. S. Renneckar, J. Saddler and F. Jiang's for access to a DSC Q1000 PerkinElmer spectrometer and C-Therm TCi™ Thermal Conductivity Analyzer.

Appendix A. Supplementary data

Supplementary data to this article can be found online at https://doi.org/10.1016/j.compositesb.2022.110231.

References

[1] Kuznik F, David D, Johannes K, Roux J-J. A review on phase change materials integrated in building walls. Renew Sustain Energy Rev 2011;15(1):379–91.
[2] Cui Y, Xie J, Liu J, Wang J, Chen. SJAiME. A review on phase change material application in building. 2017. 9(6):1687814017700828.
[3] Marani A, Nehdi ML. Integrating phase change materials in construction materials: critical review. Construct Build Mater 2019;217:36–49.
[4] Nazir H, Batool M, Bolivar Osorio FJ, Isaza-Ruiz M, Xu X, Vignarooban K, et al. Recent developments in phase change materials for energy storage applications: a review. Int J Heat Mass Tran 2019;129:491–523.
[5] Fleischer AS. Thermal energy storage using phase change materials: fundamentals and applications. Springer; 2015.
[6] Kenisarin MM. Thermophysical properties of some organic phase change materials for latent heat storage. A review. Solar Energy. 2014;107:553–75.
[7] Umair MM, Zhang Y, Iqbal K, Zhang S, Tang B. Novel strategies and supporting materials applied to shape-stabilize organic phase change materials for thermal energy storage–A review. Appl Energy 2019;235:846–73.
[8] Kuznik F, Johannes K, David D. 13 - Integrating phase change materials (PCMs) in thermal energy storage systems for buildings. In: Cabeza LF, editor. Advances in thermal energy storage systems. Woodhead Publishing; 2015. p. 325–53.
[9] Singh R, Sadeghi S, Shabani B. Thermal conductivity enhancement of phase change materials for low-temperature thermal energy storage applications. Energies 2018; 12:75.
[10] Wu S, Yan T, Kuai Z, Pan W. Thermal conductivity enhancement on phase change materials for thermal energy storage: a review. Energy Storage Mater 2020;25: 251–95.
[11] Chen Y, Zhang Q, Wen X, Yin H, Liu J. A novel CNT encapsulated phase change material with enhanced thermal conductivity and photo-thermal conversion performance. Sol Energy Mater Sol Cell 2018;184:82–90.
[12] Yang H, Chao W, Di X, Yang Z, Yang T, Yu Q, et al. Multifunctional wood based composite phase change materials for magnetic-thermal and solar-thermal energy conversion and storage. Energy Convers Manag 2019;200:112029.
[13] Zhou H, Lv L, Zhang Y, Ji M, Cen K. Preparation and characterization of a shape-stable xylitol/expanded graphite composite phase change material for thermal energy storage. Sol Energy Mater Sol Cell 2021;230:111244.
[14] Lee W, Kim J. Cellulose nanofiber grafting and aluminum nitride deposition on the surface of expanded graphite to improve the thermal conductivity and mechanical properties of phase change material composites. Compos B Eng 2022;230:109526.
[15] Yang J, Tang L-S, Bao R-Y, Bai L, Liu Z-Y, Xie B-H, et al. Hybrid network structure of boron nitride and graphene oxide in shape-stabilized composite phase change materials with enhanced thermal conductivity and light-to-electric energy conversion capability. Sol Energy Mater Sol Cell 2018;174:56–64.
[16] Mishra AK, Lahiri BB, Philip J. Carbon black nano particle loaded lauric acid-based form-stable phase change material with enhanced thermal conductivity and photo-thermal conversion for thermal energy storage. Energy 2020;191:116572.
[17] Saydam V, Duan X. Dispersing different nanoparticles in paraffin wax as enhanced phase change materials. J Therm Anal Calorim 2019;135(2):1135–44.
[18] Nourani M, Hamdami N, Keramat J, Moheb A, Shahedi M. Preparation of a stable nanocomposite phase change material (NCPCM) using sodium stearoyl lactylate (SSL) as the surfactant and evaluation of its stability using image analysis. Renew Energy 2016;93:404–11.
[19] Harikrishnan S, Kalaiselvam S. Preparation and thermal characteristics of CuO–oleic acid nanofluids as a phase change material. Thermochim Acta 2012; 533:46–55.
[20] Zhang P, Xiao X, Ma ZW. A review of the composite phase change materials: fabrication, characterization, mathematical modeling and application to performance enhancement. Appl Energy 2016;165:472–510.
[21] Chen X, Gao H, Yang M, Xing L, Dong W, Li A, et al. Smart integration of carbon quantum dots in metal-organic frameworks for fluorescence-functionalized phase change materials. Energy Storage Mater 2019;18:349–55.
[22] Wei Y, Li J, Sun F, Wu J, Zhao L. Leakage-proof phase change composites supported by biomass carbon aerogels from succulents. Green Chem 2018;20(8): 1858–65.
[23] Li Y, Huang X, Lv J, Wang F, Jiang S, Wang G. Enzymolysis-treated wood-derived hierarchical porous carbon for fluorescence-functionalized phase change materials. Compos B Eng 2022;234:109735.
[24] Raul - Augustin M, Daniela B, Cristian M. Phase change materials based on mesoporous silica. Curr Org Chem 2018;22(27):2644–63.
[25] Liu P, Gao H, Chen X, Chen D, Lv J, Han M, et al. In situ one-step construction of monolithic silica aerogel-based composite phase change materials for thermal protection. Compos B Eng 2020;195:108072.
[26] Lian Q, Li Y, Sayyed AAS, Cheng J, Zhang J. Facile strategy in designing epoxy/paraffin multiple phase change materials for thermal energy storage applications. ACS Sustainable Chem Eng 2018;6(3):3375–84.
[27] Du X, Wang S, Du Z, Cheng X, Wang H. Preparation and characterization of flame-retardant nanoencapsulated phase change materials with poly (methylmethacrylate) shells for thermal energy storage. J Mater Chem 2018;6(36): 17519–29.
[28] Huang W, Hu G, Tian C, Wang X, Tu J, Cao Y, et al. Nature-inspired salt resistant polypyrrole–wood for highly efficient solar steam generation. Sustain Energy Fuels 2019;3(11):3000–8.
[29] Wang Z, Yan Y, Shen X, Jin C, Sun Q, Li H. A wood–polypyrrole composite as a photothermal conversion device for solar evaporation enhancement. J Mater Chem 2019;7(36):20706–12.
[30] Ma L, Wang Q, Li L. Delignified wood/capric acid-palmitic acid mixture stable-form phase change material for thermal storage, vol. 194; 2019. p. 215–21.
[31] Li Y, Yu S, Chen P, Rojas R, Hajian A, Berglund L. Cellulose nanofibers enable paraffin encapsulation and the formation of stable thermal regulation nanocomposites. Nano Energy 2017;34:541–8.
[32] Meng Y, Majoinen J, Zhao B, Rojas OJ. Form-stable phase change materials from mesoporous balsa after selective removal of lignin. Compos B Eng 2020;199: 108296.
[33] Montanari Cl, Li Y, Chen H, Yan M, Berglund LA. Transparent wood for thermal energy storage and reversible optical transmittance. ACS Appl Mater Interfaces 2019;11(22):20465–72.
[34] Yang H, Chao W, Wang S, Yu Q, Cao G, Yang T, et al. Self-luminous wood composite for both thermal and light energy storage. Energy Storage Mater 2019; 18:15–22.
[35] Li J, Xue P, Ding W, Han J, Sun G. Micro-encapsulated paraffin/high-density polyethylene/wood flour composite as form-stable phase change material for thermal energy storage. Sol Energy Mater Sol Cell 2009;93(10):1761–7.
[36] Xu J, Yang T, Xu X, Guo X, Cao J. Processing solid wood into a composite phase change material for thermal energy storage by introducing silica-stabilized polyethylene glycol. Compos Appl Sci Manuf 2020;139:106098.

[37] Sun J, Zhao J, Wang B, Li Y, Zhang W, Zhou J, Guo H, Liu Y. Biodegradable wood plastic composites with phase change microcapsules of honeycomb-BN-layer for photothermal energy conversion and storage. Chem Eng J 2022:137218.
[38] Li T, Song J, Zhao X, Yang Z, Pastel G, Xu S, et al. Anisotropic, lightweight, strong, and super thermally insulating nanowood with naturally aligned nanocellulose. Sci Adv 2018;4(3):eaar3724.
[39] Qian Y, Han N, Zhang Z, Cao R, Tan L, Li W, et al. Enhanced thermal-to-flexible phase change materials based on cellulose/modified graphene composites for thermal management of solar energy. ACS Appl Mater Interfaces 2019;11(49):45832–43.
[40] Wang M, Li R, Chen G, Zhou S, Feng X, Chen Y, et al. Highly stretchable, transparent, and conductive wood fabricated by in situ photopolymerization with polymerizable deep eutectic solvents. ACS Appl Mater Interfaces 2019;11(15):14313–21.
[41] Han W, Ge C, Zhang R, Ma Z, Wang L, Zhang X. Boron nitride foam as a polymer alternative in packaging phase change materials: synthesis, thermal properties and shape stability. Appl Energy 2019;238:942–51.
[42] Chao W, Yang H, Cao G, Sun X, Wang X, Wang C. Carbonized wood flour matrix with functional phase change material composite for magnetocaloric-assisted photothermal conversion and storage. Energy 2020;202:117636.
[43] Li W, Li F, Zhang D, Bian F, Sun Z. Porous wood-carbonized solar steam evaporator. Wood Sci Technol 2021;55(3):625–37.
[44] Ren P, Li J, Zhang X, Yang X. Highly efficient solar water evaporation of TiO2@TiN hyperbranched nanowires-carbonized wood hierarchical photothermal conversion material. Mater Today Energy 2020;18:100546.
[45] Yang H, Wang Y, Yu Q, Cao G, Sun X, Yang R, Zhang Q, Liu F, Di X, Li J, Wang C. Low-cost, three-dimension, high thermal conductivity, carbonized wood-based composite phase change materials for thermal energy storage. Energy 2018;159:929–36.
[46] Wang W, Tang B, Ju B, Gao Z, Xiu J, Zhang S. Fe3O4-functionalized graphene nanosheet embedded phase change material composites: efficient magnetic- and sunlight-driven energy conversion and storage. J Mater Chem 2017;5(3):958–68.
[47] Zhu X, Li M, Song L, Zhang X-F, Yao J. Metal organic framework enabled wood evaporator for solar-driven water purification. Separ Purif Technol 2022;281:119912.
[48] Kishani S, Vilaplana F, Xu W, Xu C, Wågberg L. Solubility of softwood hemicelluloses. Biomacromolecules 2018;19(4):1245–55.
[49] Wang Z, Tang Z, Xue Q, Huang Y, Huang Y, Zhu M, et al. Fabrication of boron nitride nanosheets by exfoliation. Chem Rec 2016;16(3):1204–15.
[50] Zhou L, Yang Z, Luo W, Han X, Jang S-H, Dai J, et al. Thermally conductive, electrical insulating, optically transparent bi-layer nanopaper. ACS Appl Mater Interfaces 2016;8(42):28838–43.
[51] Yang Z, Zhou L, Luo W, Wan J, Dai J, Han X, et al. Thermally conductive, dielectric PCM–boron nitride nanosheet composites for efficient electronic system thermal management. Nanoscale 2016;8(46):19326–33.
[52] Li Y, Zhu H, Shen F, Wan J, Lacey S, Fang Z, et al. Nanocellulose as green dispersant for two-dimensional energy materials. Nano Energy 2015;13:346–54.
[53] Chen Y, Wang F, Dong L, Li Z, Chen L, He X, et al. Design and optimization of flexible polypyrrole/bacterial cellulose conductive nanocomposites using response. Surface Methodology 2019;11(6):960.
[54] Baumgärtner A, Muthukumar M. Effects of surface roughness on adsorbed polymers. J Chem Phys 1991;94(5):4062–70.
[55] Xie B, Li C, Chen J, Wang N. Exfoliated 2D hexagonal boron nitride nanosheet stabilized stearic acid as composite phase change materials for thermal energy storage. Sol Energy 2020;204:624–34.
[56] Lin L, Xu Y, Zhang S, Ross IM, Ong AC, Allwood DA. Fabrication and luminescence of monolayered boron nitride quantum dots. Small 2014;10(1):60–5.
[57] Cao C, Yang Z, Han L, Jiang X, Ji G. Study on in situ analysis of cellulose, hemicelluloses and lignin distribution linked to tissue structure of crop stalk internodal transverse section based on FTIR microspectroscopic imaging. Cellulose 2015;22(1):139–49.
[58] Duchemin B. Size, shape, orientation and crystallinity of cellulose Iβ by X-ray powder diffraction using a free spreadsheet program. Cellulose 2017;24(7):2727–41.
[59] Gong J, Li J, Xu J, Xiang Z, Mo L. Research on cellulose nanocrystals produced from cellulose sources with various polymorphs. RSC Adv 2017;7(53):33486–93.
[60] Aftab W, Mahmood A, Guo W, Yousaf M, Tabassum H, Huang X, et al. Polyurethane-based flexible and conductive phase change composites for energy conversion and storage. Energy Storage Mater 2019;20:401–9.
[61] Song M, Jiang J, Qin H, Ren X, Jiang F. Flexible and super thermal insulating cellulose nanofibril/emulsion composite aerogel with Quasi-closed pores. ACS Appl Mater Interfaces 2020;12(40):45363–72.
[62] He J, Liu S, Li Y, Zeng S, Qi Y, Cui L, et al. Fabrication of boron nitride nanosheet/polymer composites with tunable thermal insulating properties. New J Chem 2019;43(12):4878–85.
[63] Yang D, Zhou B, Han G, Feng Y, Ma J, Han J, et al. Flexible transparent polypyrrole-decorated MXene-based film with excellent photothermal energy conversion performance. ACS Appl Mater Interfaces 2021;13(7):8909–18.